Journal of Ovonic Research Vol. 14, No. 2, March - April 2018, p. 119 - 128

STRUCTURAL, MAGNETIC AND HUMIDITY SENSING PROPERTIES OF RARE EARTH DOPED COBALT FERRITE THIN FILMS SYNTHESIZED BY PULSED LASER DEPOSITION

G. BULAI[a*], O. RUSU[b], M. M. CAZACU[b,c], F. TUDORACHE[d],
B. CHAZALLON[e], C. FOCSA[e], S. GURLUI[b]
[a]*Integrated Centre for Environmental Science Studies in the North-East Development Region - CERNESIM, Alexandru Ioan Cuza University of Iasi, , Bd. Carol I, nr. 11, 700506 Iasi, Romania*
[b]*Faculty of Physics, LOA-SL, Alexandru Ioan Cuza University of Iasi, , Bd. Carol I, nr. 11, 700506 Iasi, Romania,*
[c]*Department of Physics, Gheorghe Asachi Technical University of Iasi, Bd. Mangeron 59A, Iasi, Romania*
[d]*Interdisciplinary Research Department – RAMTECH, Alexandru Ioan Cuza University of Iasi, , Bd. Carol I, nr. 11, 700506 Iasi, Romania*
[e]*PhLAM – Physique des Lasers Atomes et Molécules, Lille 1 University, CNRS, UMR 8523, F-59000 Lille, France*

Ferrites are interesting magnetic materials with a wide applicability in current and emerging technologies. $CoFe_2O_4$ presents a high magnetostrictive response, important electrical resistivity, mechanical hardness and chemical stability making this material a suitable alternative for the development of sensors, actuators and magneto-optic devices. The aim of this study was to investigate the influence of deposition conditions and rare earth substitution on the structural, magnetic and humidity sensing properties of cobalt ferrite thin films obtained by Pulsed Laser Deposition in vacuum. Preliminary results on the film thickness and uniformity were obtained by profilometry and scanning electron microscopy. Vibrational modes corresponding to cobalt ferrite were evidenced through Raman spectroscopy. Energy dispersive X-Ray analysis revealed atomic ratios close to stoichiometric ones and a uniform surface distribution of the main elements. Hysteresis loops obtained by vibrating sample magnetometry in parallel and perpendicular configurations showed no preferential magnetic ordering. Electrical resistance measurements in different relative humidity conditions (RH 0-100%) and frequencies were done using a High Frequency LCR Meter. The doped films presented a decreased electrical resistance and a lower sensitivity compared to the pure ones. This result was correlated with the structural modifications induced by the substitution of iron cations with rare earth ions.

(Received December 13, 2017; April 10, 2018)

Keywords: Cobalt ferrite; Pulsed laser deposition; Thin films; Humidity sensors

1. Introduction

The physical, electric and magnetic properties of cobalt ferrites enable their use in various types of technologies. Their application in data storage, sensors, automotive industry, microwave frequency devices and even biomedicine is due to the high corrosion resistance, good mechanical stability, moderate saturation magnetization, large magnetocrystalline anisotropy and magnetostrictive coefficient, high Curie temperature and coercive field, large permeability at high frequencies and important electrical resistivity [1-4]. Some of these properties are even more remarkable when nanostructured systems (nanoparticles, thin films) are considered and further adjustment in the structural characteristics and magnetic and electric response can be done by

*Corresponding author: georgiana.bulai@uaic.ro

changing the cation arrangement/type and synthesis process. $CoFe_2O_4$ has an inverse spinel structure $[Fe^{3+}]_A[Co^{2+}Fe^{3+}]_BO_4$ in which Co^{2+} ions occupy part of octahedral sites (B) and the Fe^{3+} ions occupy the tetrahedral sites (A) and the remaining B-sites [5]. Iron doping modifies the electronic structure of $Co_{1-x}Fe_{2+x}O_4$ thin films and can further be tailored to yield controllable resistivity changes of more than two orders of magnitude [6]. The structural modifications due to strains in Fe doped cobalt ferrite heteroepitaxial thin films led to controlled magnetic properties [7]. Sharma and Khare showed that the optical band gap and saturation magnetization can be tuned by low Zn doping [8]. The Co or Fe substitution with Mn in the spinel structure was reported to increase the saturation magnetization [9]. The enhanced reflectivity of $CoFe_{2-x}Al_xO_4$ thin film is of great interest for magneto-optical recordings [10]. Single phase multiferroic thin films based on cobalt ferrite can be obtained by Li^+-Al^{3+} pair substitution of Co^{2+} along (110) crystallographic direction [11]. The interest in rare earth doping relies on the structural and magnetic characteristics of these elements. Lanthanides present large ionic radii, different stable oxidation states and variable magnetic moments due to the partial filling of 4f shells [12]. The rare earth-Fe compounds present high magnetic anisotropies and magnetostrictions at room temperature [13]. The rare earth addition in nanostructured ferrite systems were found to enhance the magneto-optic Kerr effect [12,14], increase the cell parameter and coercive field [15,16], enlarge the saturation magnetization [17] and increase conductivity [18].

Precise humidity measurements receive great interest due to their importance in application areas such as meteorology, agriculture, automotive industry, robotics and medicine. Humidity sensors should present (among other characteristics) good thermal and chemical stability and high sensitivity. Their microstructural properties (and implicitly their synthesis method) greatly influence the humidity sensing efficiency of the system. Ferrites were found to be excellent materials for gas and humidity sensors [19-21]. Moreover, the study of Srivastava et al. revealed that in thin film form, the nickel ferrites present a higher sensitivity and a narrower hysteresis as compared to pallets or thick films [21]. However, very few results on humidity sensing properties of ferrite thin films are reported to date [22,23].

Our study was focused on the influence of the deposition conditions on cobalt ferrite thin films synthesized by Pulsed Laser Deposition (PLD), the effect of rare earth addition on the structural and magnetic properties of $CoFe_2O_4$ and analysis of the humidity sensing characteristics of the obtained samples. This was done by varying the deposition time, target-substrate distance and laser fluence and by considering three rare earth metals with different characteristics (Dy, Gd, La). The paper also presents relative humidity measurements of pure and rare earth doped cobalt ferrite thin films deposited by PLD, a topic addressed by very few research studies.

2. Experimental details

Pure and doped cobalt ferrite ($CoFe_{1.8}RE_{0.2}O_4$ [RE = Dy, Gd, La]) thin films were deposited by PLD technique using 5mm thick, 15 mm diameter disk targets. Details on the synthesis process were given in [24]. RE doped cobalt ferrite powders were obtained by solid state reaction using Fe_2O_3, Co_3O_4 and La_2O_3/Dy_2O_3/Gd_2O_3 as starting materials. The resulting powders were pressed and sintered in air for 5 hours at a temperature of 1250 °C.

For the deposition process, the as-obtained targets were placed on a multi-axis manipulator inside a stainless steel vacuum chamber where a 10^{-5} Torr pressure was ensured during the growth process. The second harmonic (532 nm) of an Nd-YAG laser (10 ns pulse width, 10 Hz repetition rate) was focused on a 1.5 mm^2 area on the target surface. The laser energy/pulse was either 30 mJ or 60 mJ, leading to fluences of 2 J/cm^2 and 4 J/cm^2, respectively. Based on the results of a previous study conducted by our group on the influence of *in-situ* substrate heating on the structural and magnetic properties of the cobalt ferrite thin films [25,26], the monocrystalline (100) silicon wafer used here as substrate was heated up to 400^{o}C by a resistive system. The target-substrate distance was varied from 40 mm to 70 mm while the deposition time was increased from 30 min (18 000 laser pulses) to 90 min (54 000 laser pulses). Considering the structural results of the pure cobalt ferrite samples, the RE doped thin films were deposited at 55 mm target-substrate

distance during 60 min with a fluence of 2 J/cm^2. The deposition parameters are summarized in Table 1.

Table 1. Deposition parameters and thicknesses of the pure and RE doped cobalt ferrite thin films.

Sample	Target	Distance (mm)	Deposition time (min)	Energy (mJ)	Thickness (nm)
C1	$CoFe_2O_4$	55	90	30	205
C2		55	60	30	120
C3		55	30	30	47
C4		55	60	60	200
C5		40	30	30	105
C6		70	30	30	22
D1	$CoFe_{1.8}Dy_{0.2}O_4$	55	60	30	120
L1	$CoFe_{1.8}La_{0.2}O_4$	55	60	30	114
G1	$CoFe_{1.8}Gd_{0.2}O_4$	55	60	30	90

The structural and chemical properties of the as-deposited thin films were investigated by various techniques. Preliminary information on the surface morphology was obtained using stylus profilometry (Veeco Dektak) and scanning electron microscopy (SEM - Vega Tescan LMH II microscope and a Bruker AXS Microanalysis GmbH detector). The chemical distribution of the constituent elements was monitored by energy-dispersive X-ray spectroscopy (EDX). Raman spectroscopy (InVia Reflex spectroscope (Renishaw), 514.5 nm excitation radiation) and X-Ray diffraction (XRD - Shimadzu LabX XRD-6000) were used to investigate the structural arrangement in the deposited material whereas magnetic measurements were performed with vibrating sample magnetometry (VSM - Princeton 3900 Model). Room temperature electrical resistivity measurements in different humidity conditions (RH0% - RH100%) and at various frequencies ranging from 20 Hz to 20 MHz were performed using a High Frequency LCR Meter (Agilent E4980A). For this type of analysis, silver electrodes were deposited on the thin film surface by thermal evaporation technique.

3. Results and discussions

3.1. Structural and magnetic properties

The thicknesses of the deposited samples obtained by profilometry are listed in Table 1. Increased thicknesses were obtained as the deposition time and laser energy were augmented and the target-substrate distance was reduced. Further analysis on the surface topography obtained by SEM revealed that all the samples presented droplets on the surface. Their density decreased as the fluence was decreased from 4 to 2 J/cm^2 (see C4 and C2) and the target substrate distance was increased to 70 mm (C6). Higher laser energies led to the ejection of large particles from the target surface. While the use of a higher target-substrate distance avoids (at least partially) their deposition on the substrate surface due to deviations from the plasma plume direction through collisions with other particles, the deposition rate is significantly diminished. In our study, the profilometry results on the thin film deposited with 70 mm target-substrate distance revealed only a 22 nm sample thickness (<1nm/min growth rate). To find a compromise between low surface roughness and acceptable deposition rate we considered that the best results were obtained for the C2 sample for which a 55 mm target-substrate distance and 30 mJ laser energy/pulse were used. Thus, the subsequent samples of RE doped cobalt ferrite were deposited in the same conditions as the pure cobalt ferrite thin film. The thickness variations between the doped and pure samples are considered to be a result of the difference between physical properties of the target which can influence the plasma plume characteristics [27]. The porosities of the $CoFe_{1.8}RE_{0.2}O_4$ targets were found to be one order of magnitude higher than those of the pure cobalt ferrite [24]. This result can explain the higher density of large droplets on the surface of the corresponding thin film.

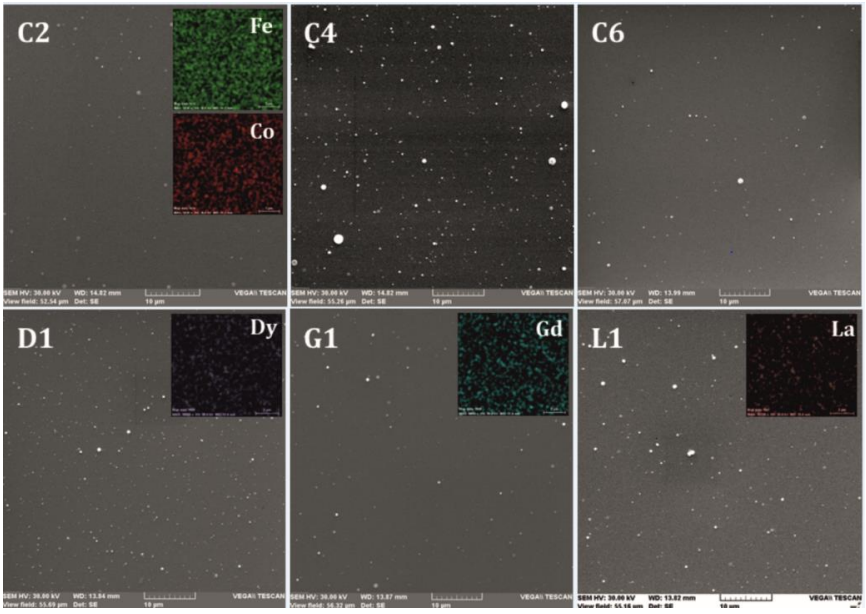

Fig. 1. SEM and EDX mapping (insets) results of several cobalt ferrite samples

Further EDX measurements revealed Fe(/FeRE):Co molar ratios close to the stoichiometric one of 2:1 for all samples and a uniform distribution of the main elements on the surface of the thin films. The deviations between the iron/cobalt concentrations and the nominal compositions were within 4% relative error (below the accuracy of the EDX). An iron deficient thin film was obtained when the target-substrate distance was set at 70 mm (C6 sample). The presence of an inter-diffusion region between the substrate and the thin film can explain the composition variations, especially when a high substrate temperature is used [28]. An inter-diffusion region was evidenced through ToF-SIMS (Time-of-Flight-Secondary Ion Mass Spectrometry) depth profiles on cobalt ferrite thin films deposited by our group in similar PLD conditions [25]. Its contribution to the structural changes in the thin film is more pronounced when very thin films are analyzed, such as C6 in our case for which only 22 nm thickness was achieved. EDX mapping of the doped samples also showed a uniform distribution of the iron, cobalt and rare earth elements (see insets on D1, G1 and L1 samples in Figure 1).

Raman spectra of the pure cobalt ferrite thin films in the 200-800 cm^{-1} spectral region are presented in Figure 2 (a). Four main peaks at 308 cm^{-1}, 460 cm^{-1}, 545 cm^{-1} and 670 cm^{-1} were observed and assigned to Raman vibrational modes of the cobalt ferrite spinel structure (O^7_h(Fd3m) space group). According to previous studies [26,29], the low-frequency modes (308 cm^{-1}, 460 cm^{-1}, 545 cm^{-1}) correspond to vibrations of the octahedral sublattice, whereas the high energy phonon mode at 670 cm^{-1} originates from vibrations of the tetrahedral sublattice. The peaks at 302 cm^{-1} and 519 cm^{-1} observed for several samples correspond to the monocrystalline silicon substrate. Its contribution to the Raman spectra is more pronounced when thinner films (such as C3 and C6) are analyzed. No frequency shifts of the cobalt ferrite Raman modes (which can indicate cation-oxygen bond length modifications) were observed from one sample to another. Thus, the varied experimental parameters (target-substrate distance, deposition time and laser energy/pulse) did not induce any internal stress or “visible” cation disorder.

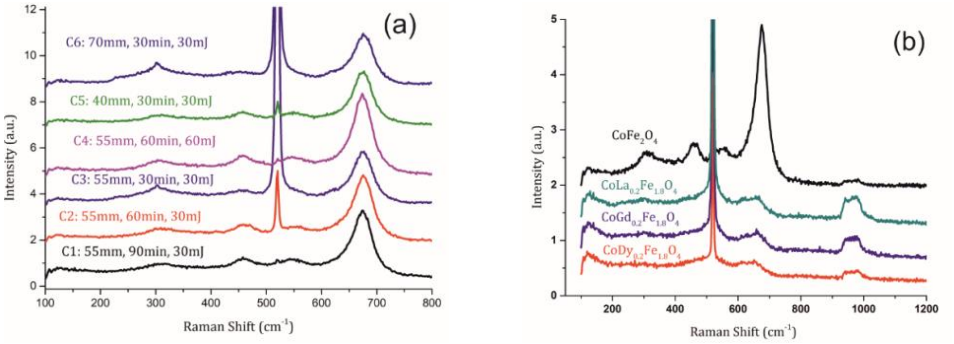

Fig. 2. Raman spectroscopy results of the pure cobalt ferrite samples (a) and doped thin films (b)

The Raman spectroscopy results of the rare earth doped thin films are presented in Figure 2 (b). Although deposited in the same conditions as the pure cobalt ferrite film, the $CoFe_{1.8}RE_{0.2}O_4$ samples presented a mixture between an amorphous phase and a crystalline structure. Previous studies on rare earth doped ferrite systems [12,14,30] and also other results reported by our group [25] showed that the addition of RE elements in the spinel structure can hinder the crystallization process and more thermal energy (either through in-situ substrate heating or subsequent thermal treatment) is needed to obtain the spinel phase compared to the stoichiometric sample. The large-radius rare earth ions are more likely to substitute the cations from the octahedral sites which can lead to lattice strains and a disordered lattice structure. Zhao et al. [29] explained the decrease in crystallite size and lattice parameters of $CoFe_{2-x}Gd_xO_4$ ferrite nanoparticles based on the larger bond energy of Gd–O compared to Fe-O (thus more energy is needed for Gd^{3+} ions to enter octahedral sites) and on the partial substitution of Fe^{3+} ion with Gd^{3+} (part of them residing at grain boundaries, further hindering their growth).

The magnetic properties of the samples were determined at room temperature by applying a 10 kOe magnetic field parallel and perpendicular to the thin film surface. The pure cobalt ferrite samples deposited in different conditions (C1-C6) presented similar hysteresis loops (not shown here) with slightly increased maximum magnetizations and coercive field observed for the C5 and C4 samples. These films were deposited using the highest laser energy and the shortest target-substrate distance, respectively. The used conditions can lead to the deposition of more energetic particles and subsequently to a higher long range crystalline order. The VSM hysteresis loops recorded for the *in-plane* configuration of the pure and RE doped samples deposited in the same conditions are plotted in Figure 3 (a). Decreased coercive fields and maximum magnetizations were found for the Gd and La doped cobalt ferrite samples while the Dy thin film presented magnetic behavior similar to the stoichiometric one. Among the three rare earth elements considered in this study, Dy has the smallest ionic radius (0.0908 nm) and the highest magnetic moment (~$10.6\mu_B$) [31]. Both characteristics enable the insertion of Dy in the octahedral sites of the spinel structure and the increase in magnetic response compared to Gd or La.

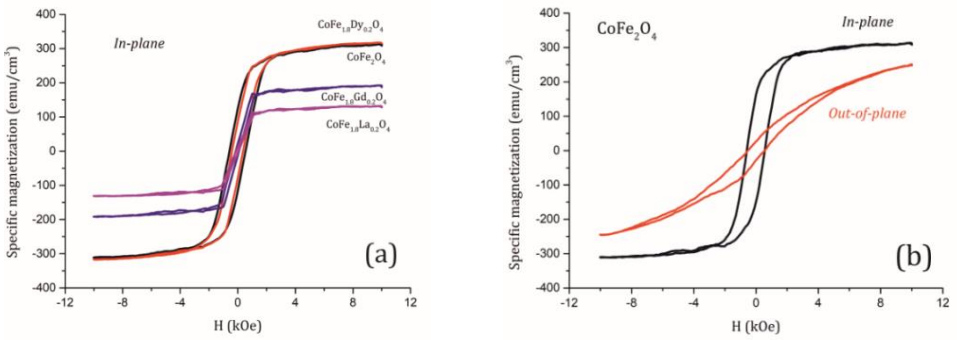

Fig. 3. VSM hysteresis loops of (a) pure and rare earth doped thin films deposited in the same conditions (In-plane configuration) and (b) $CoFe_2O_4$ sample in the in-plane and out-of-plane configurations

Figure 3 (b) presents the hysteresis loops of the C2 cobalt ferrite sample obtained in the *in-plane* and *out-of-plane* configurations. From the shape of the magnetic curves and from the similar coercive field values one can observe that there is no preferential magnetic orientation direction. The doped samples presented weak magnetic response in the out-of-plane configuration which was considered to be a result of their amorphous nature.

3.2. Humidity response

The humidity sensing characteristics of the pure and doped cobalt ferrite samples deposited in the same conditions were further analyzed. The electrical resistance frequency dependence of these samples in the relative humidity range 0–100% RH is presented in Figure 4 (a-d).

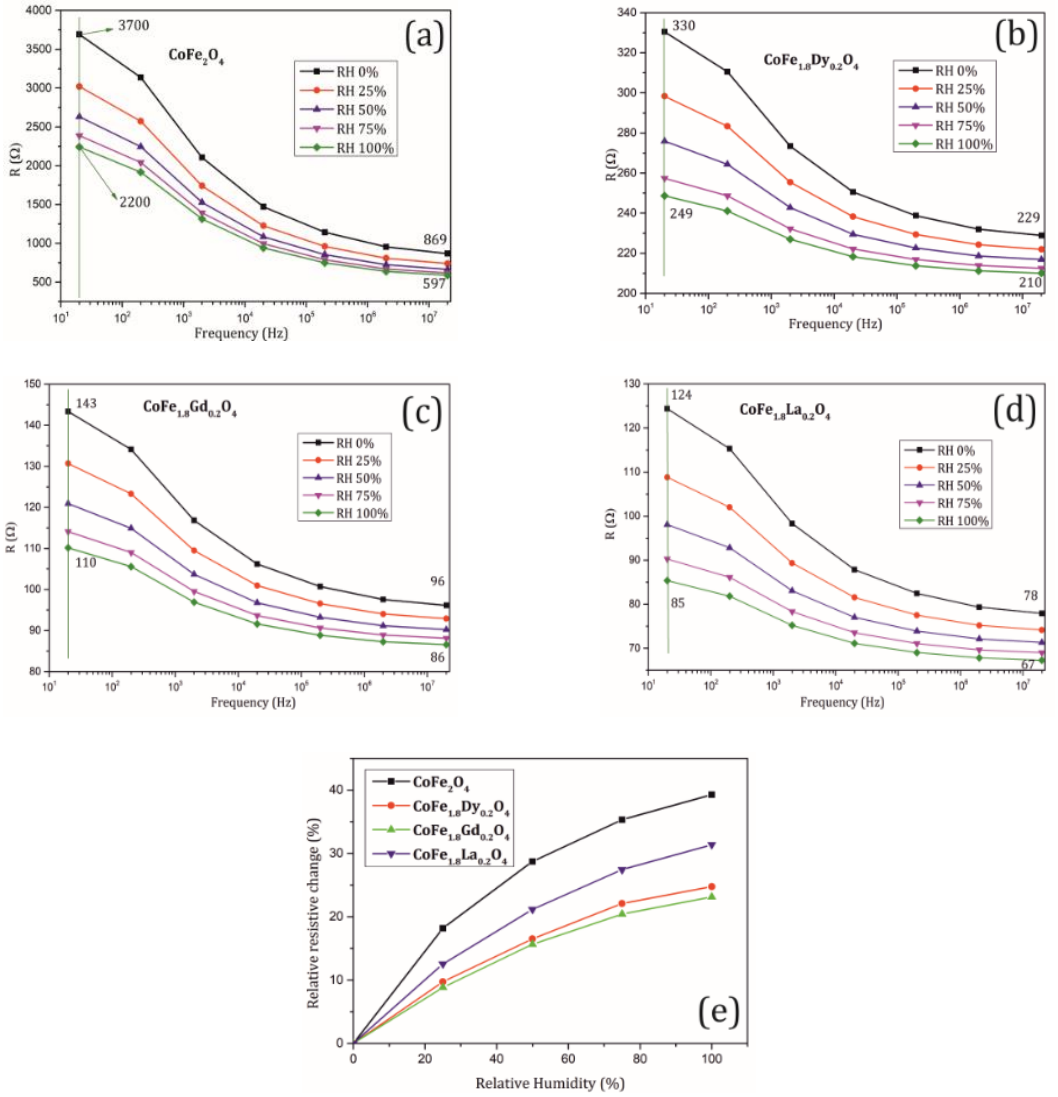

Fig. 4. Variation of electrical resistance with frequency under humidity influence at 25 °C for pure and RE doped cobalt ferrite samples (a-d) and relative resistive change of the analyzed samples (at 20 Hz) as a function of relative humidity (e).

All the analyzed samples presented a decrease of the electrical resistance as the frequency of the AC external field is increased. Conduction in ferrite samples (as in the ones from out study) can be explained by electron hopping between ions present in different valence states (Fe^{2+} - Fe^{3+}, Co^{2+} - Co^{3+}) in the octahedral sites. The frequency dependence of the AC electrical conductivity has been explained on the basis of Maxwell–Wagner model where the material is considered as being formed by a higher conductivity region, given by grains, and a lower conductivity region represented by grain boundaries. At lower frequencies the resistive grain boundaries are more active and the hopping mechanisms are hindered. When high frequency AC fields are applied, the conductive grains which promote charge carrier hopping are more active. Moreover, the addition of RE elements seems to improve the electrical conductivity of the cobalt ferrite samples analyzed in this study. The electrical resistance (at 20 Hz applied AC field and zero relative humidity) decreased as the ionic radii of the RE element increased. Similar results were reported by Farid et al. [32] and by Ahmed et al. but on different systems [33].

The electrical properties of spinel ferrites are influenced by many factors such as synthesis conditions, applied thermal treatment, density, porosity, crystallite size, grain size, exact chemical composition, type of elements present in the octahedral and tetrahedral sites and dopant concentration [34]. Haque et al. observed that the addition of La in cobalt ferrite decreased the

conductivity of the sample [35]. The number of divalent-trivalent cation pairs which cause electron hopping decreases with the replacement of Co and Fe from the octahedral sublatice with La^{3+}. However Abbas et al. obtained decreased DC electrical resistivity for the Ce doped Co-Ni ferrite pellets [36]. In their sample, Ce additions led to crystal distortion, which was considered to be the cause for the increased hopping process and net electric polarization. Similar results were reported in [37] and [18] for Gd doped cobalt ferrite. The results of Pervaiz and Gul also showed increased density (theoretical and measured) and decreased porosity, both of these properties facilitating the conduction mechanism and diminishing the electrical resistance. AC electrical conductivity measurements on Gd and Nd doped nickel ferrite reported by Mahalakshmi et al. [38] showed different results depending on the type of the RE element and its concentration. Their variations were explained by considering the electronic configuration of Nd with four unpaired electrons in the 4f orbital and Gd with only one electron in the 5d orbital which can contribute to the conductance [39]. Murugesan and Chandrasekaran found higher electrical conductivity and lower activation energies for $CoGd_xFe_{2-x}O_4$ [40]. The decrease in activation energy was attributed to the redistribution of cations due to the small particle size.

All the analyzed samples presented a decreased electrical resistance as the relative humidity was varied from 0 - 100%. The fall in resistance is due to the increased conductivity (charge carriers) upon adsorption of water vapors on the thin film surface. Ceramic humidity sensors are based on the water vapor adsorption through chemical adsorption (chemisorption), physical adsorption (physisorption) and capillary condensation processes [41]. At low humidity levels the water vapor molecules are chemisorbed on the surface of the sample. During this stage dissociative mechanisms of water vapors take place through which hydroxyl groups and protons are formed. The HO- group interacts with metal cations while the protons interact with the oxygen groups to form additional HO-. In the first chemisorbed layer, the charge transport occurs through hydrogen hopping between adjacent hydroxide ion sites. A higher surface area would have more sites for water adsorption and produce more charge carriers increasing the electric conduction [19]. As the relative humidity increases, the subsequent water vapors are physisorbed on the first formed hydroxyl layer. When more water layers are present on the sample surface, the dissociation processes that result in hydronium (H_3O^+) group formation are facilitated. In this stage the diffusion of H_3O^+ on hydroxide ions is dominant. At high humidity levels the physisorbed water molecules tend to condense in capillarity pores with radii below the Kelvin radius [42] leading to electrolytic conduction. The humidity sensing factor of the four thin films is plotted in Figure 4 (e). The doped samples presented a decrease of the relative resistance change probably due to their decreased resistance and porosity. Although the RE doped cobalt ferrite thin films presented decreased humidity sensitivity, their higher electrical conductivity (and possibly lower optical band gap values [43]) can lead to an improved photocatalytic activity. The study of Harish et al. revealed that Nd doped Ni ferrite is a promising material used for photocatalysis under natural solar light irradiation of different types of organic pollutants [44]. The photocatalytic response was correlated to its reduced band gap compared to the undoped sample. Considering also their low cost, magnetic response and environmental stability, these materials can present a large applicability domain in sensor industry.

4. Conclusions

Pure and rare earth doped cobalt ferrite thin films were deposited by laser ablation in different experimental conditions. Raman spectroscopy analysis of the $CoFe_2O_4$ samples revealed peaks corresponding to the tetrahedral and octahedral lattice vibrations. No internal stress was observed as the target-substrate distance, deposition time and laser fluence were varied. The doped samples presented a mixture between an amorphous phase and a crystalline structure. EDX mapping confirmed the presence of rare earths and the uniform distribution of the main elements on the sample surface. In-plane and out-of-plane hysteresis loops suggested that there is no preferential magnetic orientation in the $CoFe_2O_4$ thin films. Gd and La doped cobalt ferrite samples presented a weaker magnetic signal, probably due to their amorphous nature. The electrical resistance of the pure and doped samples deposited in the same conditions decreased as

the frequency of the AC field was increased. This behavior is characteristic for cobalt ferrite and was explained based on Maxwell–Wagner model. As the relative humidity was varied from 0 to 100 %, the electrical resistance of all analyzed samples decreased. The lower sensitivity of the doped samples was associated with their higher conductivity and possibly lower porosity.

Acknowledgements

This work was supported by the Romanian Space Agency (ROSA) within Space Technology and Advanced Research (STAR) Program (Project no.: 114/7.11.2016 and 169/20.07.2017).

References

[1] A. Lopez-Santiago, H.R. Grant, P. Gangopadhyay, R. Voorakaranam, R. A. Norwood, N. Peyghambarian, Opt. Mater. Express. **2**, 978 (2012).
[2] M. Djamal, Ramli, Khairurrijal, F. Haryanto, Acta Phys. Pol. A. **128**, B-19-B-23 (2015).
[3] C. Leroux, M. Bendahan, L. Ajroudi, V. Madigou, N. Mliki, Int. Meet. Chem. Sensors IMCS **2012**, 1119 (2012).
[4] M. Hussain, M. Ul-Islam, T. Meydan, Y. Melikhov, M.I. Arshad, G. Murtaza, G. Mustafa, J. Ovonic Res. **13**, 77 (2017).
[5] R. Nongjai, S. Khan, H. Ahmed, I. Khan, S. Annapoorni, S. Gautam, H.-J. Lin, F.-H. Chang, K. Hwa Chae, K. Asokan, J. Magn. Magn. Mater. **394**, 432 (2015).
[6] J. A. Moyer, C.A.F. Vaz, E. Negusse, D.A. Arena, V. E. Henrich, Phys. Rev. B - Condens. Matter Mater. Phys. **83**, 1 (2011)
[7] J.A. Moyer, D.P. Kumah, C.A.F. Vaz, D.A. Arena, V.E. Henrich, J. Magn. Magn. Mater. **345**, 180 (2013).
[8] D. Sharma, N. Khare, AIP Adv. **6**, 85005 (2016).
[9] K.J. Kim, H.K. Kim, Y.R. Park, J.Y. Park, J. Korean Phys. Soc. **49**, 1024 (2006).
[10] B. Zhou, Y.W. Zhang, C.S. Liao, Y.J. Yu, C.H. Yan, L.Y. Chen, S.Y. Wang, Appl. Phys. Lett. **82**, 1188 (2003).
[11] Y. Yu, W.-L. Li, Y.-F. Hou, T.-D. Zhang, Y. Feng, Y. Zhao, W.-D. Fei, J. Alloys Compd. **689**, 468 (2016).
[12] B. Zhou, Y.-W. Zhang, C.-S. Liao, C.-H. Yan, L.-Y. Chen, S.-Y. Wang, J. Magn. Magn. Mater. **280**, 327 (2004).
[13] A.E. Clark, AIP Conf. Proc. **18**, 1015 (1974)
[14] L. Avazpour, M.R. Toroghinejad, H. Shokrollahi, Appl. Surf. Sci. **387**, 869 (2016).
[15] Z. Karimi, Y. Mohammadifar, H. Shokrollahi, S.K. Asl, G. Yousefi, L. Karimi, J. Magn. Magn. Mater. **361**, 150 (2014).
[16] F. Cheng, C. Liao, J. Kuang, Z. Xu, C. Yan, L. Chen, H. Zhao, Z. Liu, J. Appl. Phys. **85**, 2782 (1999).
[17] C. Yan, F. Cheng, Z. Peng, Z. Xu, C. Liao, J. Appl. Phys. **84**, 5703 (1998).
[18] M.T. Rahman, M. Vargas, C.V. Ramana, J. Alloys Compd. **617**, 547 (2014).
[19] V. Jeseentharani, M. George, B. Jeyaraj, A. Dayalan, & K.S. Nagaraja, K.S. Nagaraja, J. Exp. Nanosci. **8**, 358 (2013).
[20] A. Sutka, K. Arlis, A. Gross, Sensors Actuators B. **222**, 95 (2016).
[21] R. Srivastava, B.C. Yadav, M. Singh, T.P. Yadav, J. Inorg. Organomet. Polym. Mater. **26**, 1404 (2016).
[22] R.K. Kotnala, J. Shah, R. Gupta, Sensors Actuators, B Chem. **181**, 402 (2013).
[23] R. Srivastava, N. Verma, B.C. Yadav, Adv. Sci. Lett. **20**, 917 (2014).
[24] G. Dascalu, T. Popescu, M. Feder, O.F. Caltun, J. Magn. Magn. Mater. **333**, 69 (2013).
[25] G. Dascalu, G. Pompilian, B. Chazallon, V. Nica, O.F. Caltun, S. Gurlui, C. Focsa, Appl. Phys. A. **110**, 915 (2012).
[26] G. Dascalu, G. Pompilian, B. Chazallon, O.F. Caltun, S. Gurlui, C. Focsa, Appl. Surf. Sci.

278, 38 (2013).
[27] G. Bulai, S. Gurlui, O.F. Caltun, C. Focsa, Dig. J. Nanomater. Biostructures. **10**, 1043 (2015).
[28] H. Xia, L. Lu, Y.S. Meng, Appl. Phys. Lett. **92**, 11912 (2008).
[29] X. Zhao, W. Wang, Y. Zhang, S. Wu, F. Li, J.P. Liu, Chem. Eng. J. **250**, 164 (2014).
[30] C. Yan, F. Cheng, C. Liao, J. Kuang, Z. Xu, L. Chen, H. Zhao, Z. Liu, Y. Wang, T. Zhu, G. He, J. Magn. Magn. Mater. **192**, 396 (1999).
[31] S.B. Castor, J.B. Hedrick, Rare earth elements, J. Environ. Radioact. **102**, 769 (2001).
[32] M.T. Farid, I. Ahmad, S. Aman, M. Kanwal, G. Murtaza, I. Ali, I. Ahmad, M. Ishfaq, J. Ovonic Res. **11**, 1 (2015).
[33] M. A. Ahmed, S.T. Bishay, R.M. Khafagy, N.M. Saleh, J. Magn. Magn. Mater. **350**, 73 (2014).
[34] H.S. Aziz, S. Rasheed, R.A. Khan, A. Rahim, J. Nisar, S.M. Shah, F. Iqbal, A.R. Khan, RSC Adv. **6**, 6589 (2016).
[35] S.U. Haque, K.K. Saikia, G. Murugesan, S. Kalainathan, J. Alloys Compd. **701**, 612 (2017).
[36] S.S. Abbas, I.H. Gul, S. Ameer, M. Anees, Electron. Mater. Lett. **11**, 100 (2015).
[37] E. Pervaiz, I.H. Gul, J. Phys. Conf. Ser. **439**, 12015 (2013).
[38] S. Mahalakshmi, K. SrinivasaManja, S. Nithiyanantham, J. Supercond. Nov. Magn. **27**, 2083 (2014).
[39] M.A. Ahmed, E. Ateia, S.I. El-Dek, Mater. Lett. **57**, 4256 (2003).
[40] C. Murugesan, G. Chandrasekaran, RSC Adv. **5**, 73714 (2015).
[41] H. Farahani, R. Wagiran, M.N. izar Hamidon, Sensors. **14**, 7881 (2014).
[42] K. Arshaka, K. Twomey, D. Egan, Sensors. **2**, 50 (2002).
[43] S. Benramache, O. Belahssen, A. Guettaf, A. Arif, J. Semicond. **35**, 42001 (2014).
[44] K.N. Harish, H.S. Bhojya Naik, P.N. Prashanth Kumar, R. Viswanath, ACS Sustain. Chem. Eng. **1**, 1143 (2013).